MECE E3028 Mechanical Engineering Laboratory II
Professor Qiao Lin
Spring 2022

Experiment E2: Particle Image Velocimetry

LABORATORY REPORT

Lab Group 12

Axel Ortega

Bruno Rergis

Anton Deti

Arlene Diaz

Christine Zou

Ashton Buchanan

Samuel Adeniyi

Columbia University
Department of Mechanical Engineering

March 3, 2022

Contents

Acknowledgements

Thanks to Professor Qiao Lin, as well as TAs Kechun Wen and Wenting Dai for their guidance and support throughout the experiment.

Abstract

Particle Image Velocimetry (PIV) is a high-precision optical method of flow visualization and measurement for velocity distributions within a given volume. This measurement technique is implemented in this experiment to quantitatively analyze different fluid flows. A laminar and turbulent flow are developed and characterized by their velocity profiles and Reynold's numbers; a third flow is developed in the presence of a cylinder. The analysis of the real flows were mostly consistent with the expected results in terms of the velocity profiles; the measured average axial velocity in each flow was reasonable. However, the Reynold's numbers were very inconsistent with the theoretical results.

List of Figures

List of Tables

1 Introduction

Particle Image Velocimetry (PIV) is a non-intrusive laser optical measurement technique for research and diagnostics into 3D flow visualization. A typical PIV system setup consists of tracer particles, a light source, light sheet optics, and a camera in the hardware division (1). On the software, or image analysis, side there is interrogation and post-processing. In this experiment, the objective is to measure laminar and turbulent velocity profiles as well as measuring the flow around a circular cylinder using the PIV system.

PIV was introduced in the late 1970s and is now known as a standard measurement technique in fluid mechanics. Studying Particle Image Velocimetry is important because of the usefulness of the system. One being, that it is a quantitative flow field mapping technique that can provide physical insight into the overall flow behavior in question. Another advantage being that the system facilitates both the visualization of the fluid flow as well as the measurement data (2). These advantages are displayed during this experiment as the team identified the laminar, turbulent, and circular cylinder flow using PIV.

2 Theory

2.1 PIV Principle

Particle Image Velocimetry (PIV) is an optical method of flow visualization and measurement for velocity distributions in spatial regions (3). This method utilizes imaging techniques to perform image analysis on a cross-section of a flow. More specifically, the velocity vectors in a fluid flow are obtained via tracking the movement of small particles seeded in the flow, accomplished by analyzing photographic images of the particles at two time instants (4).

Tracer particles are added to a fluid and illuminated in a plane of flow twice (4). A camera is used to image this area and capture each light pulse in separate image frames(3). After at least two light pulses or frames are recorded, the images are split into subsections known as interrogation areas (IAs) (3). These areas are then cross correlated with each other, as an indicator of match goodness (3). By performing this cross-correlation analysis for each IA of the first frame, a velocity vector map over the entire target area is obtained. A schematic of the general setup of a PIV can be seen in Fig. 1 (3).

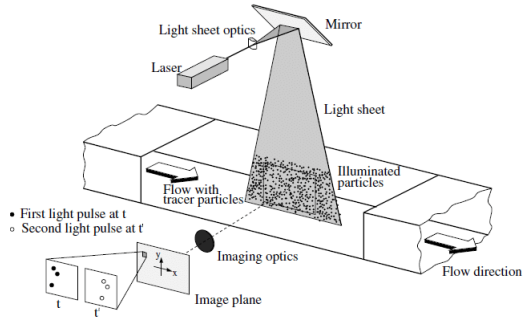

Figure 1: PIV Experimental Setup

2.1.1 Cross-Correlation

After two frames are collected and divided into small interrogation regions (IAs), the displacement of particles within one small region is computed. This region is then matched with a region in frame 2 using cross-correlation (3). The process entails locating a correlation box in one frame, or IA of interest, and conducting a search in the second frame using a correlation box of the same size (3). This process can be seen in Fig. 2.

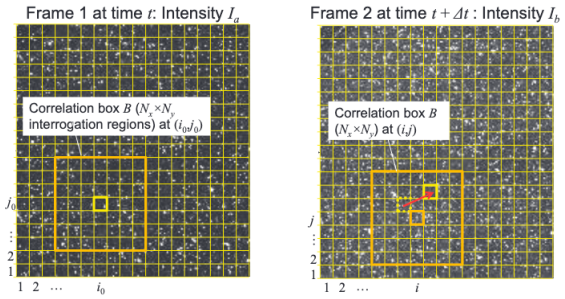

Figure 2: Interrogation regions in frame 1 and frame 2.

In order to compute the displacement of particles in the IA, the intensity of the IA in frame 2, I_b, at location (i, j) is cross-correlated with the intensity of the IA in frame 1, I_a, at location (i_0, j_0) (3). This computation is performed by constructing two functions that are zero-normalized over the correlation interval and denote the image intensities in both frames (3). Eq. 1 and 2 denote these two functions as average light intensities in correlation box B at locations (i_0, j_0) and (i, j) for I_a and I_b, respectively.

$$\bar{I}_a = \frac{1}{N_x N_y} \sum_{(k,l) \in B} I_a(k, l) \tag{1}$$

$$\bar{I}_b = \frac{1}{N_x N_y} \sum_{(k,l) \in B} I_b(k, l) \tag{2}$$

The cross correlation between I_a within B at (i_0, j_0) and I_b within B at (i, j) is given by the following equation (3):

$$\Phi_{(i_0,j_0)}(i, j) = \frac{\sum_{(k,l) \in B} (I_a(k, l) - \bar{I}_a)(I_b(k, l) - \bar{I}_b)}{(\sum_{(k,l) \in B} (I_a(k, l) - \bar{I}_a)(I_b(k, l) - \bar{I}_b))^{\frac{1}{2}}} \tag{3}$$

The location where the light intensities of both IA regions best match is yielded by the location that maximizes the cross-correlation function in Eq. 3 (3). After cross-correlating these IAs from both frames, a signal peak is produced and used calculate the average particle displacement, Δx (3). The velocity of the particles in these IAs can also be found using the average particle displacements.

2.2 Laminar Flow

2.2.1 Laminar Flow Velocity Profile in an Incompressible Fluid Flow

To determine the velocity profile for a fully-developed laminar flow in an incompressible fluid flow channel, the Navier-Stokes equation as outlined in Appendix A.1.1 and continuity equation for an incompressible Newtonian fluid with constant viscosity are used (5). The continuity equation for a steady, incompressible Newtonian fluid with uniform density ρ and constant viscosity μ is defined as (5):

$$\frac{\partial u}{\partial x} + \frac{\partial v}{\partial y} + \frac{\partial w}{\partial z} = 0 \tag{4}$$

Assuming a fully-developed flow between two parallel plates separated by thickness h with velocity only varying in the x direction, $v = v(x)$, the Navier-Stokes equation in the y direction is derived:

$$\rho\left(u\frac{\partial v}{\partial x} + v\frac{\partial v}{\partial y} + w\frac{\partial v}{\partial z}\right) = -\frac{\partial p}{\partial y} + \mu\left(\frac{\partial^2 v}{\partial x^2} + \frac{\partial^2 v}{\partial x^2} + \frac{\partial^2 v}{\partial x^2}\right) + \rho g_y \tag{5}$$

The u and w components are both 0, as v only varies with x. This simplifies the continuity equation to yield:

$$\frac{\partial v}{\partial y} = 0 \tag{6}$$

and the Navier-Stokes equation becomes:

$$0 = -\frac{\partial p}{\partial y} + \mu\left(\frac{\partial^2 v}{\partial x^2}\right) + \rho g_y \tag{7}$$

After rearranging this equation, integrating both sides twice with respect to x, applying the no slip boundary condition at $x = \pm h/2$, where v=0, and solving for constants C_1 and C_2, a solution $v(x)$ is found.

$$v(x) = \frac{1}{\mu}\left(\frac{x^2}{2} - \frac{h^2}{8}\right)\left[\rho g_y + \frac{\partial p}{\partial y}\right] \tag{8}$$

This equation can be simplified further to yield:

$$v = \frac{G}{8\mu}(h^2 - 4x^2) \tag{9}$$

where $G = -\rho g_y - \frac{\partial p}{\partial y}$ is a constant that represents the combined effect of gravity and pressure gradient along channel of fluid flow (6). Integrating Eq. 9 over a cross section of the channel yields the following equation for volumetric flow rate Q:

$$Q = \int_A v\, dA \; = \frac{GL}{R_0} \tag{10}$$

where A is the channel cross-sectional area and $R_0 = 12\mu L/bh^3$ is the **flow resistance** of the channel. Eq. 9 can then be rewritten as the velocity profile in terms of volumetric flow as

$$v = \frac{3Q}{2bh}\left[1 - 4\left(\frac{x}{h}\right)^2\right]. \tag{11}$$

This shows that a laminar and incompressible flow has a parabolic velocity profile.

2.2.2 Effective Pressure Drop

The continuity and Navier-Stokes equations from the previous section can be used to show that velocity is in the channel's axial (x) direction. In addition, pressure p varies only with x, meaning $p = p(x)$ and $\frac{dp}{dx} =$ constant (6).

For a fully-developed laminar flow, the equivalent pressure drop is defined by $\Delta p_e ff = GL$, where $G = \rho g_x - \frac{dp}{dz}$ denotes the equivalent pressure gradient (6). Plugging these back in for pressure drop over a channel experiencing laminar flow yields:

$$\Delta p_{eff} = \left(\rho g_x - \frac{dp}{dz}\right) H \tag{12}$$

The equivalent pressure drop for the channel in the PIV experimental apparatus becomes simply $\rho g \Delta Z$, as the channel is vertical and only experiencing a hydrostatic pressure drop due to gravity (6). ΔZ represents the entire channel length $L + H$, which gives

$$GL = \rho g(L + H) - p_e \tag{13}$$

where p_e denotes the pressure difference of the value in the apparatus (6).

2.2.3 Shear Stress and Total Shear Force on Channel Walls

The flow exerts a shear stress on the channel walls as it travels. For a laminar flow of a Newtonian fluid, the shear stress τ_w is proportional to the velocity gradient:

$$\tau_w = \mu \frac{du}{dy} \tag{14}$$

Using conservation of momentum in a control volume with area $A = bh$ and perimeter $S = 2(b + h)$ the shear stress in a laminar flow can be determined (6):

$$\tau_w \left(\frac{SL}{A}\right) = \rho g(L + H) - p_e \tag{15}$$

Since the shear stress is in units of force per unit area, the total shear force on the channel walls exerted by the flow can be found using the surface area of the channel walls, which yields a result in units of Newtons.

$$F_{shear} = \tau_w \times A_{surface} \tag{16}$$

where A is the area of the four walls in the pipe that span length L.

2.2.4 Flow Resistance

For a well developed laminar flow in a thin rectangular channel with negligible gravity effects, $G = \frac{\Delta p}{L}$. Recalling flow rate Q and that $\Delta p = p_1 - p_2$ (6):

$$Q = \frac{Gbh^3}{12\mu} = \frac{bh^3}{12\mu L}\Delta p \tag{17}$$

Using the electrical analogy for fluid flow in pipes, the flow resistance of the value in the PIV apparatus can be determined (6). Let Δp = voltage, Q = current, and R = electrical resistance. Combining the 'voltage' and 'current' can help yield 'electrical resistance' R (6). The flow resistance R can, thus, be rewritten as:

$$R = \frac{\Delta p}{Q} = \frac{12\mu L}{bh^3} \tag{18}$$

For this experiment, the PIV apparatus consists of a reservoir of height H and a channel of height L. The setup can be seen in Fig. 3.

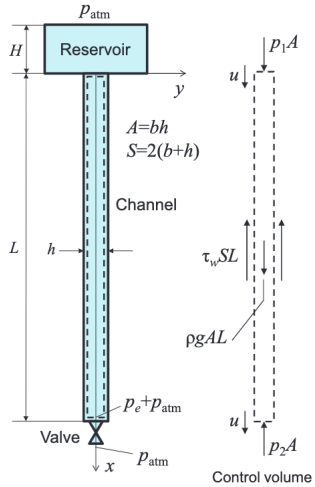

Figure 3: Labeled Schematic of PIV Experimental Apparatus

For the schematic shown in Fig. 3, $\Delta Z_{AB} = L$, and $\Delta p_{AB} = (\rho g H + p_{atm}) - (p_e + p_{atm})$. Note that $p_e = R_v Q$, where R_v is the flow resistance of the valve (6). p_e represents the total hydrostatic pressure drop through the apparatus (6). This is shown on Fig. 3 as the total equivalent pressure drop from reservoir water level to exit. Since the flow is driven by this pressure drop, the following equation is used:

$$GL = \rho g \left(\Delta Z_{AB} + \frac{\Delta p_{AB}}{\rho g} \right) \tag{19}$$

After substituting in for ΔZ_{AB} and Δp_{AB}, combining Eq. 10 and Eq. 19, and solving for flow rate Q, the following equation is derived:

$$Q = \left(1 + \frac{H}{L}\right)\left(1 + \frac{R_v}{R_0}\right)^{-1}\left(\frac{\rho g L}{R_0}\right) \tag{20}$$

In the case where the valve flow resistance exceeds that of the channel ($R_v >> R_0$), the flow rate can be simplified to:

$$Q = \frac{\rho g\,(L + H)}{R_v} \tag{21}$$

2.3 Turbulent Flow

2.3.1 Turbulent Flow Velocity Profile in Incompressible Fluid Flow

Turbulence is a fluid flow in which fluid motion is characterized by chaotic changes in pressure and flow velocity (which can be seen by the disruptions between parallel layers in fluid flows) (7). Turbulent flow has a "fuller" velocity profile than laminar flow near a solid wall due to the strong energy exchange between fluid particles (5). This means that the velocity gradient for turbulent flow near a solid wall is larger than the velocity gradient for laminar flow near a solid wall. The mean velocity and mean pressure for a steady turbulent flow are denoted by Eq. 22 and Eq. 23, respectively (5).

$$\bar{v} = \frac{1}{T}\int_0^T v(t)dt \tag{22}$$

$$\bar{p} = \frac{1}{T}\int_0^T p(t)dt \tag{23}$$

where T denotes a sufficiently long time duration. When calculating turbulent flow, the effects of the side walls of a channel are negligible, just as in the case for laminar flow. This is due to the channel depth being much larger than the channel thickness. Since the calculations for turbulent flow in this experiment entail mean pressure and mean velocity, the Navier-Stokes and continuity equations do not apply, as they deal with instantaneous pressure and velocity (6).

Assuming a fully-developed and incompressible fluid flow between two parallel plates of distance h, the turbulent velocity profile can be found using power law (8):

$$U = u_{max}\left(\frac{\frac{h}{2} - y}{\frac{h}{2}}\right)^{\frac{1}{n}} = u_{max}\left(\frac{h - 2y}{h}\right) \tag{24}$$

where u_{max} is the velocity at the center of the channel. Integrating Eq. 24 over the entire cross-section yields an average flow velocity U in terms of u_{max} as

$$U = \frac{2n^2}{(n+1)(2n+1)}u_{max} \tag{25}$$

By rearranging Eq. 25, the turbulent velocity profile is obtained as,

$$u = \frac{(n+1)(2n+1)}{2n^2}\left(\frac{Q}{bh}\right)\left[1-2\left(\frac{y}{h}\right)\right]^{\frac{1}{n}} \tag{26}$$

where the exponent $\frac{1}{n}$ is a function of Reynold's number (8). This profile can also be derived using logarithmic law, which expresses the profile in terms of wall shear stress (8).

Reynold's number for the channel is defined by:

$$Re = \frac{\rho U h}{\mu} = \frac{U h}{\nu} \tag{27}$$

where U is the average velocity across the channel width, h, and where ρ, μ and ν are the density, dynamic viscosity and kinematic viscosity of water, respectively (8).

2.3.2 Effective Pressure Drop

$$GL = \rho g h_f \tag{28}$$

2.3.3 Shear Stress and Total Shear Stress on Channel Walls

$$\tau_w = \frac{f}{8}\rho V^2 \tag{29}$$

where f is the friction factor, and V the average velocity (6). To find the friction factor, the Colebrook formula or Haaland formula can be used (6). In this experiment, the Haaland equation is used to obtain the Darcy friction factor using $D_{\text{eff}} = \frac{2D_h}{3}$ and $D_h = \frac{2bh}{b+h}$:

$$\frac{1}{f^{\frac{1}{2}}} \approx -1.8\log\left[\left(\frac{\frac{\varepsilon}{D_{\text{eff}}}}{3.7}\right)^{1.11} + \frac{6.9}{Re_{D_{\text{eff}}}}\right]. \tag{30}$$

2.3.4 Flow Resistance

Based on the equivalent pressure drop over the channel described previously, the following equation gives the flow resistance through the channel, R_0T

$$GL = QR_{0T} \approx \rho g(L+H)(\frac{R_{0T}}{R_v}) \tag{31}$$

2.4 Entrance Effects in Channel Flow

An inviscid upstream flow converges and enters the entrance region of a channel as shown in Fig 4. The changes in the velocity profiles as the flow travels can be seen here. Viscous boundary layers grow downstream, retarding the axial flow at the wall and accelerating the center core flow (6). At the entrance, viscous effects and velocity changes are significant (9). Once flow is in the fully-developed region, velocity does not change with the axial coordinate (6).

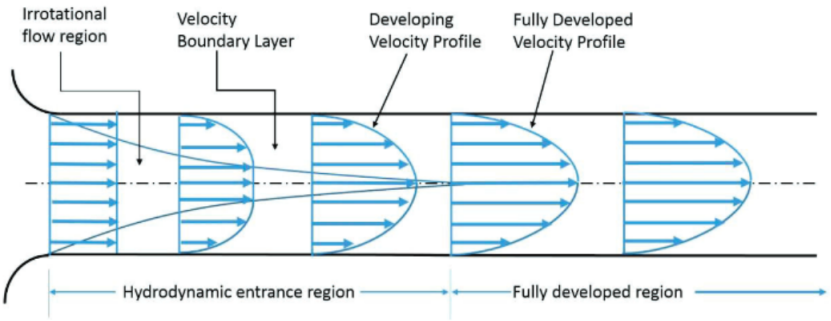

Figure 4: Entrance Region for a Pipe Flow

The entrance length L_e for a laminar flow is found with Eq. 32 (6).

$$L_e = d0.06Re_d \tag{32}$$

For a turbulent flow, with the condition that $Re_d \leq 10^7$, the entrance length is found as:

$$L_e \approx dRe_d^{0.25} \tag{33}$$

where $d = 2h$ and Re_d is determined using Eq. 27 (6).

2.5 Potential Flow Theory

Potential flow is an idealized model of fluid flow that occurs in the case of incompressible, inviscid, and irrotational flow (8). The velocity potential of a potential flow satisfies Laplace's equation:

$$\nabla^2 \vec{\phi} = 0 \tag{34}$$

Potential flow theory describes the velocity field as the gradient of a scalar function, which is referred to the velocity potential. Potential flows can be used to describe both incompressible and compressible flows.

2.6 Flow Around a Circular Cylinder

In the case of a uniform stream past a circular cylinder of radius a and infinite length, the potential flow is expressed in terms of a scalar function governed by the Laplace equations:

$$v_r = U\cos\theta(1 - \frac{a^2}{r^2}) \tag{35}$$

$$v_\theta = -U\sin\theta(1 + \frac{a^2}{r^2}) \tag{36}$$

By applying boundary conditions at the cylindrical surface for this inviscid and irrotational flow, the velocity distribution is found as

$$v_r = 0 \tag{37}$$

$$v_\theta = -2U \sin\theta \tag{38}$$

To find the pressure on the surface of the cylinder, Bernoulli's equation outlined in Appendix A.1.2 and the velocity distribution from equations 37 and 38 can be used. This pressure on the surface is derived as:

$$p_s = p_\infty + \frac{1}{2}\rho U^2(1 - 4\sin^2\theta) \tag{39}$$

3 Apparatus and Approach

This experiment uses a camera, a laser, and several tubes through which water flows. These components are used to then analyze the fluid flow on a particle scale by using Dantec Dynamic Studio Software - which utilizes a single camera to measure two velocity components in a plane.

The laser illuminates particles within the fluid flow through the water channel. This light that hits the particles is then scattered and picked up by the high speed camera. The position and movements of the particles are thereby observable and traceable through these frames.

Figure 5: Camera

Figure 6: Laser driver

Figure 7: Laser source

3.1 Apparatus

The apparatus of the experiment consists of a few different key elements. The water channels for fluid flow analysis using Dynamic Studio are key; the structure is shown in Fig. 8. The following are the dimensions for individual components of structure: Reservoir has dimensions of 12in x 12in x 12in (height, width, depth); Channel 1 has dimensions of 74in x 0.53in x 4in (height, width, depth); Channel 2 has dimensions 74in x 1.575in x 4in (height, width, depth); and the cylinder is 0.375in in diameter.

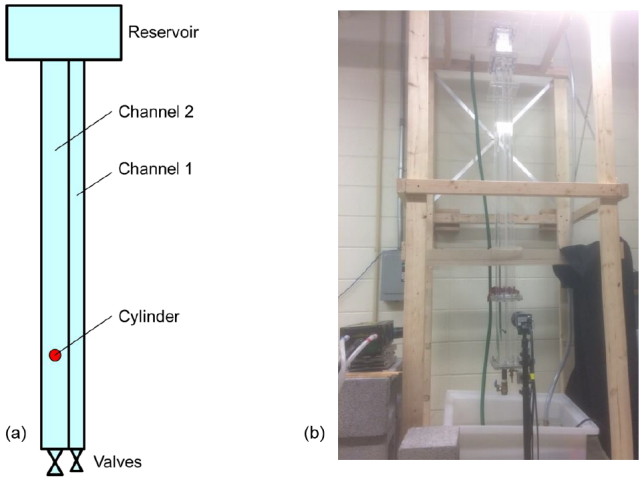

Figure 8: Vertical fluid channels structure, (a) schematic and (b) built structure

3.2 Approach

The flow in the tubes must first be calibrated. This is done by measuring the amount of water that has flown in a given time scale. The lower valve controls when the flow starts and stops and the upper valve adjusts flow rate and should only be used when the lower valve is closed. These measurements can be put together to calculate different Reynolds numbers for Channels 1 and 2.

For this experiment, the Dynamic Studio Software will be used. Once it is started, under the "Run" menu, "Enter acquisition mode" should be selected and then the laser will not turn on. At this point it is important to always wear laser safety glasses. In order to turn the laser beam on, under the "View" menu in "System Control," "Free Run", "Preview", and "Acquire" will turn it on.

Ensure the camera captures a clear image of microparticles in the measurement region of the channel by adjusting the location and focus of it. By using "Preview", the camera can be adjusted until satisfactory. Submerge a ruler into the tank, and use "Acquire Data" to capture an image for calibration. With the image, under "Calibration", use the "Measure Scale Factor" to then calibrate the software to correlate pixel length to actual length. The value that is input should be that of the channel wall because of the known dimensions of the channel wall; if the channel wall is not within view, adjust the camera so that the channel wall is in frame.

Parameters under "System Control" must be adjusted; the options are "Time between pulses", "Trigger Rate", and "Number of images". The only parameter that must be adjusted is "Time between pulses" which acts as the time between each image that is captured; within the pulse time, particles should move less than half of a full square on the grid that the software overlays onto the image of the fluid flow.

With the "Acquire" option in "system Control", obtain videos of microparticles in the water flow. Save these videos. Right-click on the video and select "Adaptive PIV", "Apply", then "OK" for the software to begin analyzing. Export the data, and then repeat for all

videos. The images that were collected should be analyzed natively within the Dynamic Studio Software using "Image Mean" (creates average image) and "Image Arithmetic" (removes background noise). After, "Adaptive PIV" should be used on top of "Image Arithmetic" to find a velocity profile of the flow.

The velocity profile in Channel 1 with Reynolds numbers of 400 and 800, based on channel width, will be measured respectively. The velocity profile, away from the cylinder, in Channel 2 will also be measured at Reynolds numbers of 4,000 and 5,000 along with the velocity distributions, near the cylinder, at these Re numbers. Finally, the Reynolds number defined using the cylinder diameter will be computed.

4 Results

4.1 Average Velocity and Relevant Reynolds Number Values

The experiment yielded different axial velocities and different Reynold's numbers for each flow. These are tabulated in Table 1. The data used to generate these values according to Eq. 27 can be found in Appendix A.2. Typical velocity profiles can be found in Fig. 9 through Fig. 16.

Flow	Average Axial Velocity (m/s)	Reynold's Number for Average Axial Velocity
Laminar Flow	-0.007316	98.264
Turbulent Flow	-0.4595	18341
Cylinder Flow	-0.4246	16945

Table 1: Average Axial Velocities in Each Flow and Corresponding Reynold's Numbers

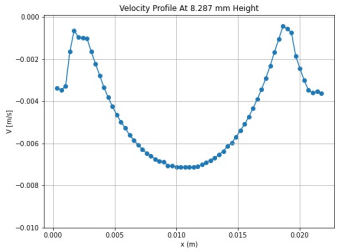

Figure 9: Uncropped Velocity Plot of Laminar Flow at 8.287 mm Height

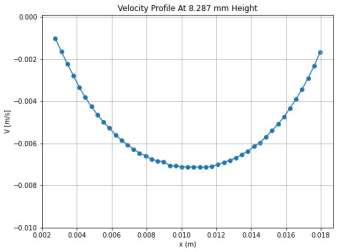

Figure 10: Cropped Velocity Plot of Laminar Flow at 8.287 mm Height

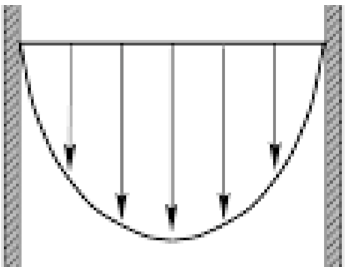

Figure 11: Ideal Velocity Plot for Laminar Flow

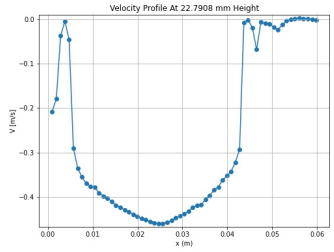

Figure 12: Uncropped Velocity Plot of Turbulent Flow at 22.7908 mm Height

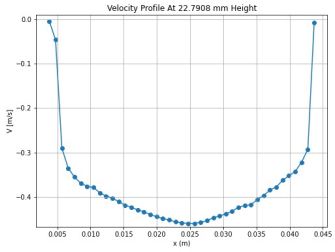

Figure 13: Cropped Velocity Plot of Turbulent Flow at 22.7908 mm Height

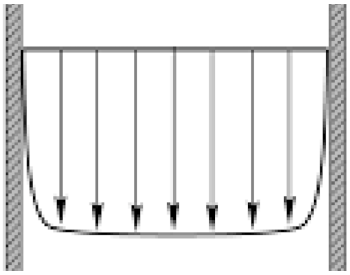

Figure 14: Ideal Velocity Plot for Turbulent Flow

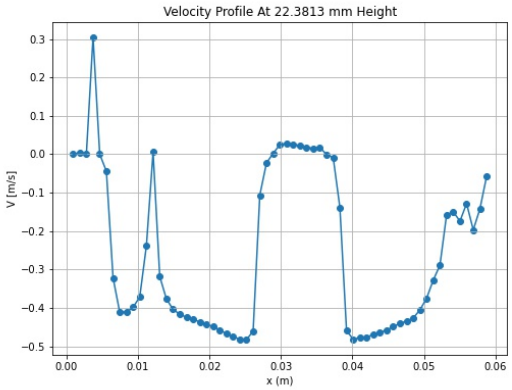

Figure 15: Uncropped Velocity Plot of Flow in Presence of Cylinder at 8.389 mm Height

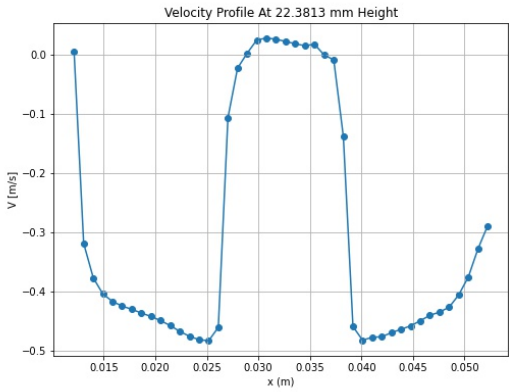

Figure 16: Cropped Velocity Plot of Flow in Presence of Cylinder at 8.389 mm Height

4.2 Parameters for Laminar Flow

4.2.1 Effective Pressure Drop Through Channel

The effective pressure drop through Channel 1 is 3.47 Pa.

4.2.2 Shear Stress and Total Shear Force on Channel Walls

$D_{\text{h}} = 0.01538\text{m}$ and $D_{\text{eff}} = 0.0102533\text{m}$, using Channel 1 cross-sectional dimensions: $b = 0.04\text{m}$ and $h = 0.009525\text{m}$. Using the Darcy friction factor as well as the average axial velocity for turbulent flow V, the shear stress obtained is $0.4358\ \frac{N}{m^2}$. The shear force obtained is 0.0364 N.

4.3 Parameters for Turbulent Flow

4.3.1 Effective Pressure Drop Through Channel

The effective pressure drop through Channel 2 is 393.46 Pa.

4.3.2 Shear Stress and Total Shear Force on Channel Walls

$D_{\text{h}} = 0.0574\text{m}$ and $D_{\text{eff}} = 0.03826\text{m}$, using Channel 2 cross-sectional dimensions: $h = 0.04\text{m}$ and $b = 0.1016\text{m}$. Using the Darcy friction factor given by the Haaland equation, as well as the average axial velocity for turbulent flow V, the shear stress obtained is 4.0045 $\frac{N}{m^2}$. The shear force obtained is 0.1924 N.

4.3.3 Flow Resistance

Through the use of Equation (34) we can obtain the flow resistance.

We can determine from this set of data that for the turbulent flow the Flow Resistance is 22572 Pa s/m^3

4.4 Flow past cylinder

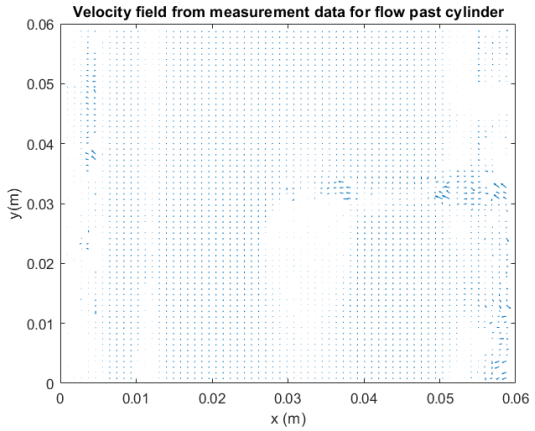

Figure 17: Vector velocity plot for measured flow past cylinder

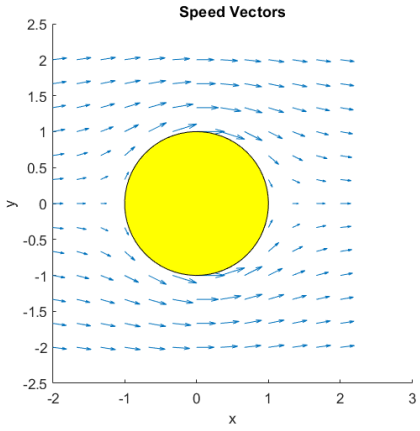

Figure 18: Vector velocity plot using the solution for a flow past cylinder

4.5 Quality

The velocity plots for the measured laminar and turbulent flow resemble the ideal velocity plots of these flows very closely. So, we can assume for these two objectives of the experiment, the results we obtained are reasonable because of the consistency to the ideal charts. The velocity plot for the flow in the presence of the cylinder neither resembles turbulent or laminar

flow or anywhere in between. This makes it hard to finalize that our results are reasonable along with the idea there isn't an ideal velocity flow chart for this certain situation.

5 Discussion

Due to the questionable set up of the experiment, it is unclear if the experiment was performed correctly. The Reynold's numbers for each flow are not unreasonable for the phenomena being recorded: laminar flow, turbulent flow, and flow in the presence of a cylinder. However, these values are not consistent with the expected values. The laminar flow measurements were originally intended to be measured with a flow with a Reynold's number between 400 and 500 and the turbulent flow measurements were originally intended to be measured with a flow with a Reynold's number between 4,000 and 5,000.

It is unlikely that extraneous data is the source of this inconsistency. To clarify: the PIV laser setup recorded data in excess of the width of either tube and created extraneous data in all flows. These were cropped from the data sets in Appendix A.2 when calculating the values in Table 1. Extraneous values were removed to include only values that were within the expected internal width of the tube. Plots of the respective vertical velocities within the flow at a constant height were compared and are shown in Fig. 9 through Fig. 16. The cropped velocity profiles in Fig. 10 and Fig. 13 are consistent with the theoretical velocity profiles in Fig. 11 and Fig. 14 respectively.

However, even when taking into account that the Reynold's numbers were calculated using the average minimum velocity at a given height as measured by the PIV's lasers, the Reynold's numbers are still far too high for the turbulent flow and the flow in the presence of the cylinder. Water level in the reservoir affected the results as the raw data indicated more irregular flow on experimental attempts where the water level was lower.

When examining Fig. 18, the yellow circle is meant to illustrate the cylinder in the flow. As seen in the vector plot, the velocity flows clearly around it. However, when analyzing Fig. 17, while there seems to be some areas where the flow is flowing around the object, it is significantly harder to identify where the cylinder is, because the setup is not perfect. It seems that the cylinder could potentially be near 0.03 m in the x-direction, and 0.02-0.03 m in the y-direction, however there are other notable disruptions in the flow between the 0.05-0.06 m in the x-direction. Nonetheless, this could simply be due to imperfections in the experimental setup.

6 Conclusions

Three flows were analyzed and characterized using a PIV setup. Velocity distributions within each flow were reasonable however the Reynold's number calculated from mean velocities via the PIV measurements were largely inconsistent with the expected values for each flow. Analysis of the flows were limited by the angle of the placement of the PIV system relative to the fluid flow. The PIV clearly measured flow data outside the channel as seen in Fig. 9, Fig.

12, and Fig. 15; fluid does not move significantly when adjacent to walls therefore velocities that were detected past the main curve that demonstrated the velocity profile within the flow belonged to fluid flow outside the intended scope of the experiment. This issue was further compounded by the small, finite number of data points available within each frame of the PIV's camera. Precision was therefore lost when calculating Reyonld's numbers due to the need for removing extraneous data points that were not associated with the flow itself. Because these pre-processed data sets did not always include near-zero values for velocity at the channel boundaries and instead began and ended at arbitrary, non-zero and non near-zero values, the boundary phenomena within the channels is not well characterized.

Overall the results of the analyses of the flows was consistent with theoretical results in terms of the general shape of the velocity profiles. However, the Reynold's numbers pertaining to each flow deviated significantly from the expected values. The experiment should be retested carefully with a different experimental setup to verify the results in this experiment to determine the sources of the discrepancies.

References

[1] D. Dynamics, "Particle image velocimetry," 2021.

[2] Y. Huang, "Particle image velocimetry," 2021.

[3] Q. Lin, "Particle image velocimetry principle and experiment," 2022.

[4] M. e. a. Kelnberger, "Particle Image Velocimetry: Basics, Developments and Techniques," *Photonics Marketplace*.

[5] Q. Lin, "External flow review: Incompressible fluid flow around a solid body," 2022.

[6] Q. Lin, "Internal flow review: Incompressible viscous fluid flow in pipes," 2022.

[7] "Turbulence," 2014.

[8] Q. Lin, "Particle image velocimetry laboratory," 2022.

[9] "Entrance length (fluid dynamics),"

Contributions by section:

- Abstract: Bruno
- Introduction: Ashton
- Theory: Arlene, Axel
- Apparatus and Approach: Christine
- Results: Bruno, Anton, Christine, Ashton, Sam, Axel
- Discussion: Bruno, Christine, Ashton, Axel, Sam
- Conclusions: Bruno
- Appendix: Bruno

A Appendix

A.1 Relevant Equations

A.1.1 Navier-Stokes Equation (in scalar form) for steady, incompressible flow

$$\rho\left(u\frac{\partial u}{\partial x}+v\frac{\partial u}{\partial y}+w\frac{\partial u}{\partial z}\right)=-\frac{\partial p}{\partial x}+\mu\left(\frac{\partial^2 u}{\partial x^2}+\frac{\partial^2 u}{\partial x^2}+\frac{\partial^2 u}{\partial x^2}\right)+\rho g_x$$

$$\rho\left(u\frac{\partial v}{\partial x}+v\frac{\partial v}{\partial y}+w\frac{\partial v}{\partial z}\right)=-\frac{\partial p}{\partial y}+\mu\left(\frac{\partial^2 v}{\partial x^2}+\frac{\partial^2 v}{\partial x^2}+\frac{\partial^2 v}{\partial x^2}\right)+\rho g_y$$

$$\rho\left(u\frac{\partial w}{\partial x}+v\frac{\partial w}{\partial y}+w\frac{\partial w}{\partial z}\right)=-\frac{\partial p}{\partial z}+\mu\left(\frac{\partial^2 w}{\partial x^2}+\frac{\partial^2 w}{\partial x^2}+\frac{\partial^2 w}{\partial x^2}\right)+\rho g_z$$

A.1.2 Bernoulli's Equation for steady, inviscid, and incompressible flow

$$\nabla\left(p+\frac{1}{2}\rho V^2+\rho g y\right)=\rho\bar{v}\times\bar{\Omega}$$

A.2 Data Used in Calculations

y (m)	Average U (m/s)	Min V (m/s)	Average Speed (m/s)	Reynold's Number
0.34012	-7.4786E-04	-8.9641E-03	7.8609E-03	120.39642
0.68564	-1.4793E-03	-1.0955E-02	7.5773E-03	147.13248
1.03115	-1.2274E-03	-1.0055E-02	6.8386E-03	135.04487
1.37667	-6.0553E-04	-7.1645E-03	5.9752E-03	96.22517
1.72219	-3.7071E-05	-7.1585E-03	5.4601E-03	96.14539
2.06771	-5.7351E-05	-7.1715E-03	5.4359E-03	96.32043
2.41322	-4.7212E-05	-7.1600E-03	5.3728E-03	96.16478
2.75874	-5.0176E-05	-7.1677E-03	5.3784E-03	96.26863
3.10426	-5.6488E-05	-7.1513E-03	5.3545E-03	96.04829
3.44978	-5.3898E-05	-7.1463E-03	5.3756E-03	95.98155
3.79529	-5.3828E-05	-7.1198E-03	5.3420E-03	95.62489
4.14081	-4.9822E-05	-7.1012E-03	5.3500E-03	95.37551
4.48633	-5.0174E-05	-7.1389E-03	5.3503E-03	95.88237
4.83185	-4.9444E-05	-7.1534E-03	5.3462E-03	96.07606
5.17736	-4.9914E-05	-7.1529E-03	5.3452E-03	96.06947
5.52288	-4.8896E-05	-7.1385E-03	5.3560E-03	95.87668
5.86840	-4.3553E-05	-7.1569E-03	5.3399E-03	96.12403
6.21392	-4.4180E-05	-7.1687E-03	5.3511E-03	96.28260
6.55943	-3.9439E-05	-7.1688E-03	5.3493E-03	96.28311

6.90495	-4.1216E-05	-7.1836E-03	5.3501E-03	96.48286
7.25047	-4.7505E-05	-7.1468E-03	5.3422E-03	95.98817
7.59598	-4.2127E-05	-7.1429E-03	5.3362E-03	95.93520
7.94150	-4.4272E-05	-7.1272E-03	5.3318E-03	95.72478
8.28702	-4.6696E-05	-7.1315E-03	5.3292E-03	95.78198
8.63254	-4.9991E-05	-7.1739E-03	5.3336E-03	96.35245
8.97805	-4.8962E-05	-7.1711E-03	5.3417E-03	96.31487
9.32357	-4.8598E-05	-7.1790E-03	5.3471E-03	96.42110
9.66909	-4.4349E-05	-7.1737E-03	5.3360E-03	96.34973
10.01461	-4.2864E-05	-7.1741E-03	5.3424E-03	96.35482
10.36012	-3.9643E-05	-7.1762E-03	5.3447E-03	96.38354
10.70564	-4.4194E-05	-7.1561E-03	5.3481E-03	96.11280
11.05116	-5.2422E-05	-7.1346E-03	5.3478E-03	95.82427
11.39668	-5.4730E-05	-7.1455E-03	5.3531E-03	95.97113
11.74219	-4.9052E-05	-7.1663E-03	5.3453E-03	96.24947
12.08771	-4.7480E-05	-7.1776E-03	5.3577E-03	96.40230
12.43323	-4.6434E-05	-7.1807E-03	5.3416E-03	96.44371
12.77875	-5.1226E-05	-7.1938E-03	5.3470E-03	96.61879
13.12426	-4.5955E-05	-7.1839E-03	5.3722E-03	96.48694
13.46978	-4.7096E-05	-7.2083E-03	5.3693E-03	96.81396
13.81530	-5.0654E-05	-7.1903E-03	5.3715E-03	96.57286
14.16082	-5.0111E-05	-7.1918E-03	5.3618E-03	96.59184
14.50633	-4.1257E-05	-7.1831E-03	5.3793E-03	96.47497
14.85185	-3.6229E-05	-7.2108E-03	5.3850E-03	96.84828
15.19737	-4.0048E-05	-7.2174E-03	5.3843E-03	96.93653
15.54289	-4.2049E-05	-7.2181E-03	5.3812E-03	96.94631
15.88840	-4.8499E-05	-7.1971E-03	5.3663E-03	96.66369
16.23392	-5.2992E-05	-7.2128E-03	5.3578E-03	96.87499
16.57944	-5.5171E-05	-7.2193E-03	5.3656E-03	96.96121
16.92496	-5.5259E-05	-7.2221E-03	5.3877E-03	96.99884
17.27047	-5.4509E-05	-7.2281E-03	5.3786E-03	97.07996
17.61599	-5.0403E-05	-7.2394E-03	5.3694E-03	97.23243
17.96151	-5.0840E-05	-7.2144E-03	5.3672E-03	96.89571
18.30703	-5.0441E-05	-7.1856E-03	5.3584E-03	96.50875
18.65254	-4.9531E-05	-7.1972E-03	5.3589E-03	96.66519
18.99806	-4.3712E-05	-7.2151E-03	5.3608E-03	96.90549
19.34358	-4.3279E-05	-7.2169E-03	5.3612E-03	96.92953
19.68909	-4.6555E-05	-7.2082E-03	5.3618E-03	96.81340
20.03461	-4.7002E-05	-7.2230E-03	5.3692E-03	97.01121
20.38013	-4.4530E-05	-7.2467E-03	5.3642E-03	97.33008

20.72565	-4.6188E-05	-7.2348E-03	5.3725E-03	97.16990
21.07116	-4.5101E-05	-7.2548E-03	5.3823E-03	97.43843
21.41668	-4.8266E-05	-7.2458E-03	5.3919E-03	97.31721
21.76220	-4.3117E-05	-7.2336E-03	5.5121E-03	97.15374

Table 2: Laminar Flow Processed Data

y (m)	Average U (m/s)	Min V (m/s)	Average Speed (m/s)	Reynold's Number
0.93539	8.3194E-04	-4.5505E-01	3.8526E-01	18162.3245
1.88562	1.7743E-03	-4.5556E-01	3.8600E-01	18182.6849
2.83586	1.3853E-03	-4.5297E-01	3.8560E-01	18079.322
3.78609	8.1778E-04	-4.5311E-01	3.8556E-01	18084.8542
4.73633	8.8628E-05	-4.5270E-01	3.8361E-01	18068.5302
5.68656	-2.5794E-04	-4.5201E-01	3.8423E-01	18040.9182
6.63680	-9.9601E-04	-4.5153E-01	3.8131E-01	18021.8377
7.58704	-1.4058E-03	-4.5075E-01	3.8362E-01	17990.4273
8.53727	-2.1742E-03	-4.5003E-01	3.8516E-01	17962.0683
9.48751	-2.0776E-03	-4.5268E-01	3.8354E-01	18067.5426
10.43774	-1.3772E-03	-4.5181E-01	3.8262E-01	18032.7802
11.38798	-1.4275E-03	-4.4981E-01	3.8419E-01	17953.1638
12.33821	-3.5842E-04	-4.4935E-01	3.8272E-01	17934.7917
13.28845	2.4534E-04	-4.4904E-01	3.8301E-01	17922.5548
14.23868	5.6443E-04	-4.4935E-01	3.8380E-01	17934.836
15.18892	7.6777E-04	-4.5135E-01	3.8096E-01	18014.6466
16.13915	5.5613E-04	-4.5345E-01	3.8307E-01	18098.2782
17.08939	1.5419E-04	-4.5450E-01	3.7987E-01	18140.344
18.03962	-1.1347E-04	-4.5475E-01	3.7944E-01	18150.1176
18.98986	-3.9889E-04	-4.5421E-01	3.7781E-01	18128.7261
19.94009	1.8739E-04	-4.5707E-01	3.7833E-01	18242.958
20.89033	2.7070E-04	-4.5773E-01	3.7899E-01	18269.226
21.84057	2.2987E-04	-4.5735E-01	3.7817E-01	18254.196
22.79080	-3.1612E-04	-4.5907E-01	3.7773E-01	18322.7728
23.74104	-5.1164E-04	-4.6214E-01	3.7771E-01	18445.4083
24.69127	-5.1847E-04	-4.6238E-01	3.7770E-01	18454.628
25.64151	-7.3773E-04	-4.6345E-01	3.8000E-01	18497.3855
26.59174	-6.5625E-04	-4.6359E-01	3.8067E-01	18503.1072
27.54198	-2.6947E-04	-4.6221E-01	3.8139E-01	18447.9748
28.49221	-1.0559E-04	-4.6270E-01	3.8137E-01	18467.7364
29.44245	-1.8695E-05	-4.6309E-01	3.8197E-01	18483.1614
30.39268	-5.3768E-04	-4.6211E-01	3.8187E-01	18444.0377
31.34292	-8.0185E-04	-4.6211E-01	3.8075E-01	18444.1682
32.29315	-2.1269E-04	-4.6062E-01	3.8033E-01	18384.6555
33.24339	1.0113E-04	-4.6072E-01	3.7989E-01	18388.3972
34.19362	5.4576E-04	-4.6149E-01	3.7989E-01	18419.2796
35.14386	1.3847E-03	-4.6065E-01	3.7940E-01	18385.7818
36.09410	7.8137E-04	-4.6082E-01	3.7900E-01	18392.4196

37.04433	1.3554E-03	-4.6222E-01	3.7527E-01	18448.4434
37.99457	8.4859E-04	-4.6279E-01	3.7492E-01	18470.9774
38.94480	7.3996E-04	-4.6262E-01	3.7393E-01	18464.342
39.89504	2.8030E-05	-4.6152E-01	3.7094E-01	18420.3951
40.84527	-7.0319E-04	-4.6223E-01	3.6783E-01	18448.9851
41.79551	-1.1825E-03	-4.6013E-01	3.6625E-01	18365.022
42.74574	-1.2915E-03	-4.6129E-01	3.6598E-01	18411.3344
43.69598	-1.8930E-03	-4.6061E-01	3.6536E-01	18384.3204
44.64621	-1.3319E-03	-4.6083E-01	3.6637E-01	18393.0938
45.59645	-1.1521E-03	-4.5934E-01	3.6665E-01	18333.3155
46.54668	-6.3433E-04	-4.5847E-01	3.6682E-01	18298.8887
47.49692	-5.0809E-04	-4.5886E-01	3.6666E-01	18314.3546
48.44716	-9.6343E-05	-4.5865E-01	3.6657E-01	18305.9489
49.39739	6.9612E-05	-4.5894E-01	3.6593E-01	18317.3318
50.34763	-1.2523E-04	-4.5835E-01	3.6607E-01	18294.1057
51.29786	-1.7054E-04	-4.5883E-01	3.6615E-01	18313.0231
52.24810	-4.1417E-05	-4.5965E-01	3.6656E-01	18345.859
53.19833	4.3280E-04	-4.5944E-01	3.6613E-01	18337.5278
54.14857	2.8463E-04	-4.5857E-01	3.6643E-01	18302.5867
55.09880	5.1644E-04	-4.5901E-01	3.6664E-01	18320.3546
56.04904	-1.1993E-03	-4.5945E-01	3.6705E-01	18338.0297
56.99927	-1.6526E-03	-4.5990E-01	3.6664E-01	18355.974
57.94951	3.7964E-04	-4.5991E-01	3.6572E-01	18356.3113
58.89974	1.9664E-04	-4.5907E-01	3.6693E-01	18322.6032
59.84998	-1.5307E-02	-5.6698E-01	3.6637E-01	22629.504

Table 3: Turbulent Flow Processed Data

y (m)	Average U (m/s)	Min V (m/s)	Average Speed (m/s)	Reynold's Number
0.91858	2.7815E-04	-4.0745E-01	3.0656E-01	16262.215
1.85175	2.6947E-03	-4.0481E-01	3.0241E-01	16157.108
2.78491	5.5624E-04	-3.9768E-01	3.0485E-01	15872.486
3.71807	2.7765E-03	-4.0385E-01	3.0927E-01	16118.546
4.65123	1.5152E-03	-4.0176E-01	3.0554E-01	16035.153
5.58440	-1.7912E-03	-4.0663E-01	3.0852E-01	16229.796
6.51756	-3.7446E-03	-4.0347E-01	3.1143E-01	16103.404
7.45072	-1.2574E-04	-4.0740E-01	3.1168E-01	16260.544
8.38389	-2.2061E-03	-4.1212E-01	3.1119E-01	16448.626
9.31705	-1.6807E-03	-4.1637E-01	3.1135E-01	16618.253
10.25021	-5.8544E-03	-4.1813E-01	3.0788E-01	16688.830
11.18338	-7.4004E-03	-4.2274E-01	3.1228E-01	16872.656
12.11654	-8.2579E-03	-4.2465E-01	3.1069E-01	16948.975
13.04970	-1.0048E-02	-4.3292E-01	3.1912E-01	17278.964
13.98286	-1.0031E-02	-4.4244E-01	3.2329E-01	17658.858
14.91603	-8.2219E-03	-4.5215E-01	3.2676E-01	18046.402
15.84919	-3.7289E-03	-4.6055E-01	3.1961E-01	18381.795
16.78235	8.2138E-04	-4.7074E-01	3.1786E-01	18788.562
17.71552	6.1973E-04	-4.7785E-01	3.2558E-01	19072.283
18.64868	-1.1797E-03	-4.8108E-01	3.2380E-01	19201.034
19.58184	1.3405E-03	-4.8123E-01	3.2124E-01	19207.132
20.51501	-7.2134E-04	-4.8269E-01	3.1995E-01	19265.344
21.44817	-2.2901E-03	-4.8094E-01	3.1812E-01	19195.653
22.38133	-3.2456E-03	-4.8317E-01	3.0684E-01	19284.605
23.31449	-2.3404E-03	-4.8663E-01	3.0309E-01	19422.839
24.24766	-1.6521E-03	-4.9002E-01	2.9610E-01	19558.022
25.18082	-1.4462E-03	-4.8814E-01	2.9214E-01	19483.019
26.11398	-8.3395E-05	-4.8919E-01	2.9084E-01	19524.748
27.04715	-1.8088E-03	-4.8958E-01	2.8702E-01	19540.472
27.98031	-4.5013E-03	-4.8537E-01	2.8748E-01	19372.450
28.91347	-2.8187E-02	-4.9556E-01	2.4243E-01	19779.021
29.84664	-1.1352E-02	-4.7150E-01	2.7374E-01	18818.684
30.77980	-1.1748E-01	-5.8477E-01	3.8557E-01	23339.594
31.71296	-1.6189E-01	-4.5793E-01	3.8488E-01	18277.108
32.64612	-1.2344E-01	-7.2652E-01	4.3561E-01	28997.421
33.57929	-6.3811E-02	-5.8427E-01	4.2019E-01	23319.812
34.51245	-1.7133E-02	-8.6524E-01	4.3171E-01	34533.910
35.44561	5.6970E-03	-4.3493E-01	3.2070E-01	17359.313

36.37878	-5.3575E-03	-3.8117E-01	3.0333E-01	15213.494
37.31194	-1.7890E-04	-3.7545E-01	3.0598E-01	14985.205
38.24510	-5.7796E-04	-3.7205E-01	2.9999E-01	14849.637
39.17827	-1.3639E-03	-3.6742E-01	2.9959E-01	14664.664
40.11143	-1.3969E-03	-3.6229E-01	2.9740E-01	14460.104
41.04459	-1.1940E-03	-3.5746E-01	2.9640E-01	14267.125
41.97775	-1.5034E-03	-3.5323E-01	2.9917E-01	14098.425
42.91092	-1.8150E-03	-3.4900E-01	3.0079E-01	13929.434
43.84408	-1.8728E-03	-3.4547E-01	3.0198E-01	13788.601
44.77724	-1.7745E-03	-3.4305E-01	3.0131E-01	13692.226
45.71041	-2.1466E-03	-3.4042E-01	2.9859E-01	13587.025
46.64357	-2.8937E-03	-3.3914E-01	2.9743E-01	13536.164
47.57673	-3.1296E-03	-3.3782E-01	2.9764E-01	13483.213
48.50989	-3.2429E-03	-3.3644E-01	2.9692E-01	13428.336
49.44306	-3.2457E-03	-3.3461E-01	2.9431E-01	13355.159
50.37622	-2.8329E-03	-3.3615E-01	2.9451E-01	13416.735
51.30938	-2.9168E-03	-3.4011E-01	2.9517E-01	13574.553
52.24255	-3.2182E-03	-3.3733E-01	2.9617E-01	13463.739
53.17571	-3.5357E-03	-3.3990E-01	2.9708E-01	13566.234
54.10887	-4.0028E-03	-3.4080E-01	2.9704E-01	13602.125
55.04204	-3.9115E-03	-3.4164E-01	2.9672E-01	13635.748
55.97520	-3.8768E-03	-3.4444E-01	2.9700E-01	13747.477
56.90836	-3.9274E-03	-3.4472E-01	2.9787E-01	13758.584
57.84152	-3.9737E-03	-3.4579E-01	2.9968E-01	13801.486
58.77469	-4.5151E-03	-3.5990E-01	3.0217E-01	14364.485

Table 4: Cylinder Flow Processed Data

A.3 Minimum Vertical Velocity in Flows

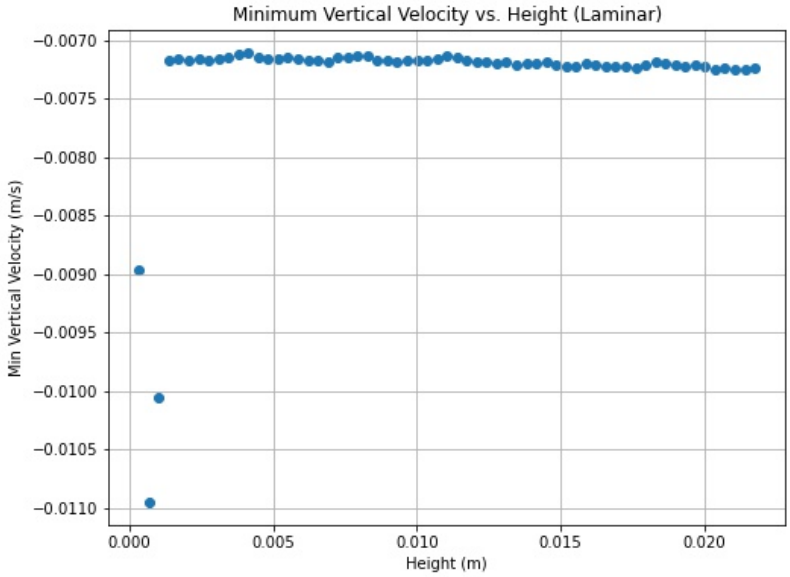

Figure 19: Minimum Vertical Velocity in Laminar Flow with Respect to Height

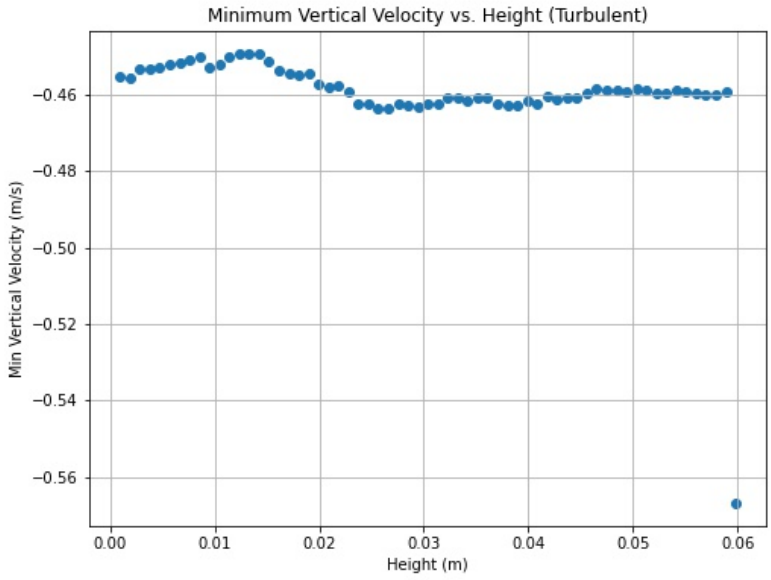

Figure 20: Minimum Vertical Velocity in Turbulent Flow with Respect to Height

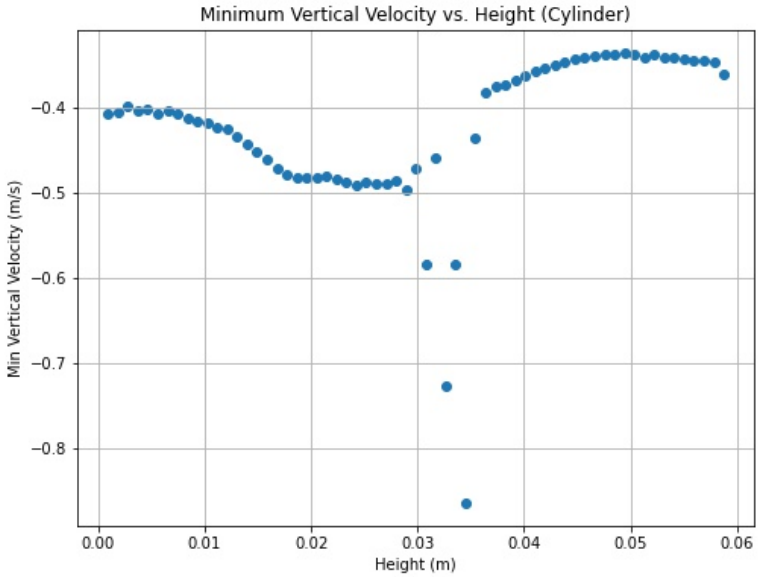

Figure 21: Minimum Vertical Velocity in Cylinder Flow with Respect to Height

A.4 Reynold's Numbers in Flows

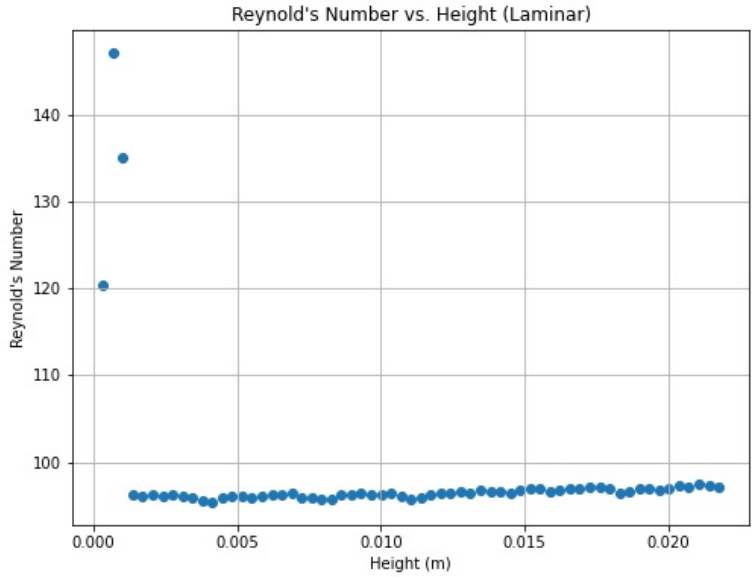

Figure 22: Reynold's Number in Laminar Flow with Respect to Height

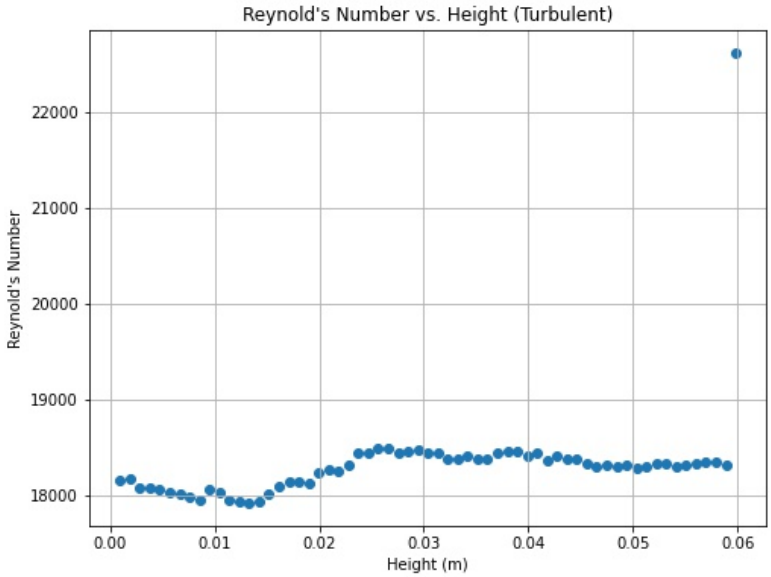

Figure 23: Reynold's Number in Turbulent Flow with Respect to Height

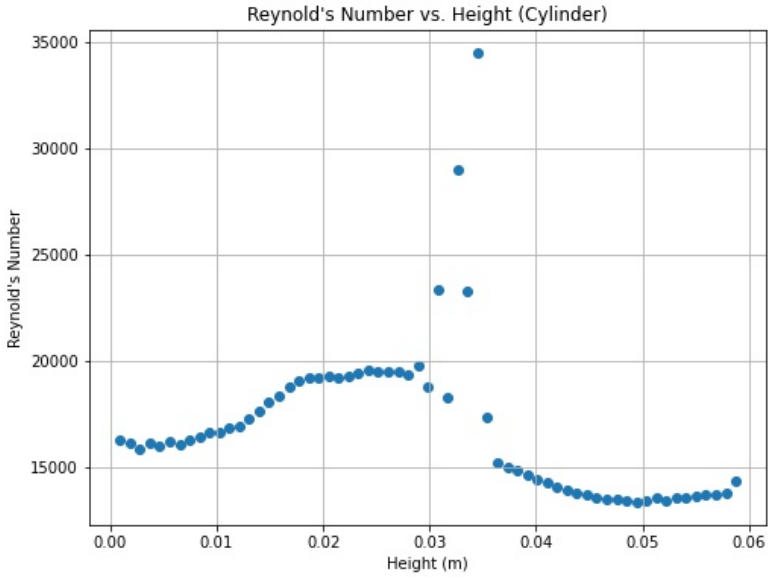

Figure 24: Reynold's Number in Cylinder Flow with Respect to Height

A.5 Average Horizontal Velocity in Flows

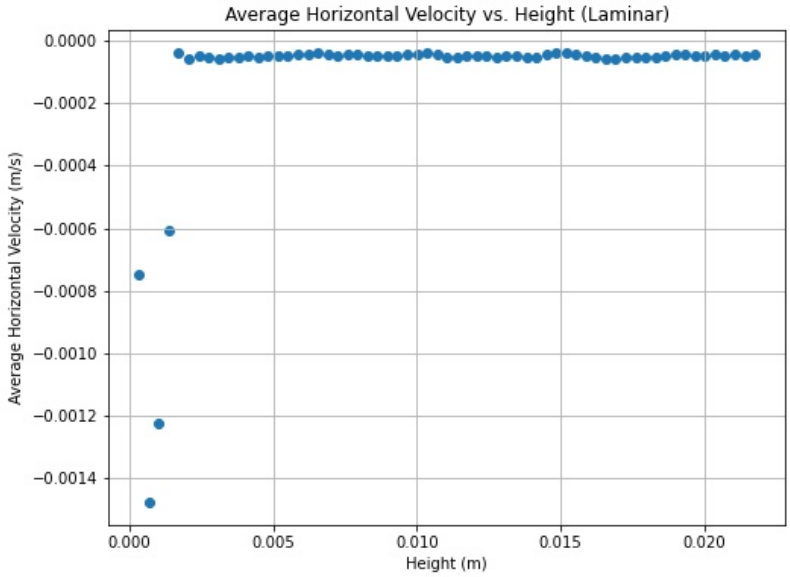

Figure 25: Average Horizontal Velocity in Laminar Flow with Respect to Height

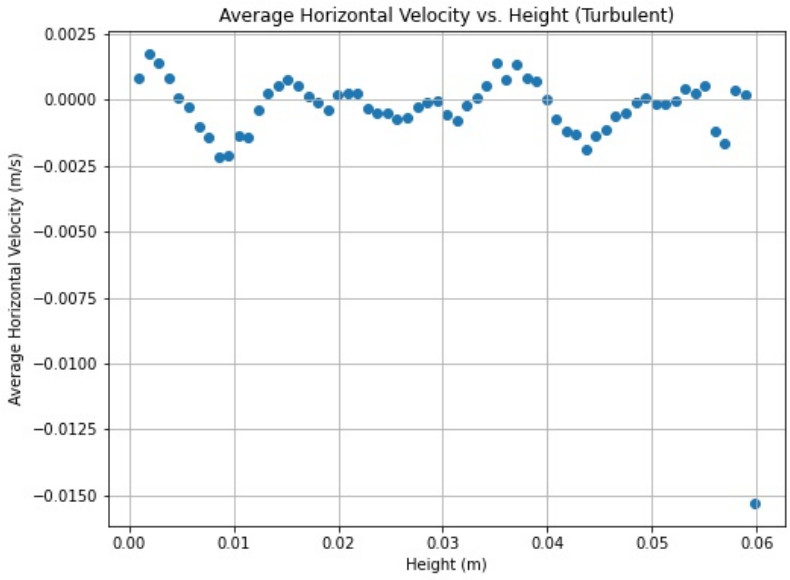

Figure 26: Average Horizontal Velocity in Turbulent Flow with Respect to Height

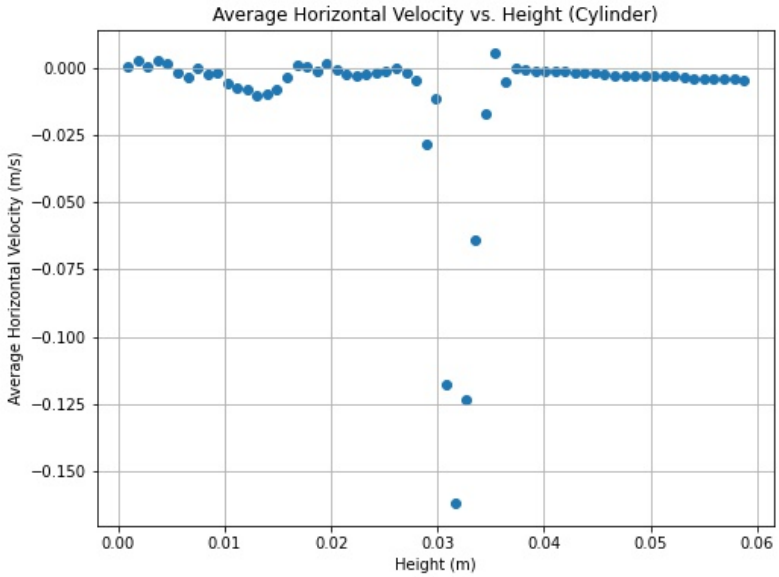

Figure 27: Average Horizontal Velocity in Cylinder Flow with Respect to Height

A.6 Average Speeds in Flows

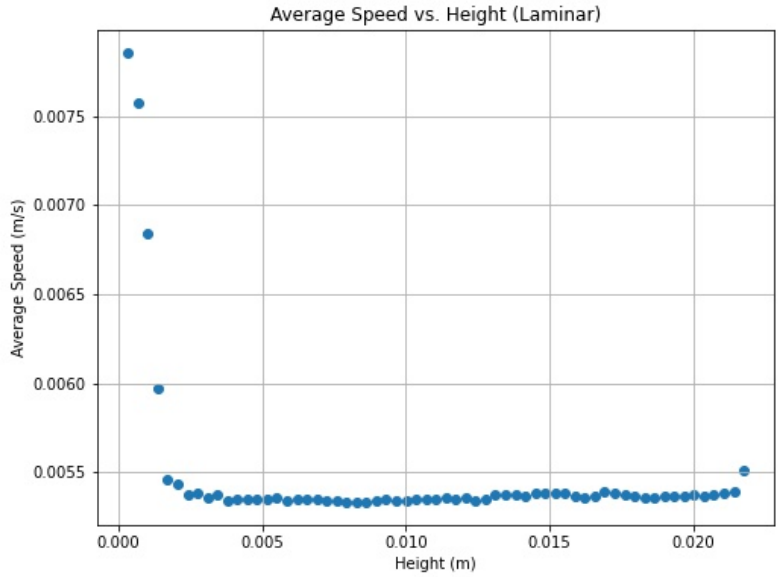

Figure 28: Average Speed in Laminar Flow with Respect to Height

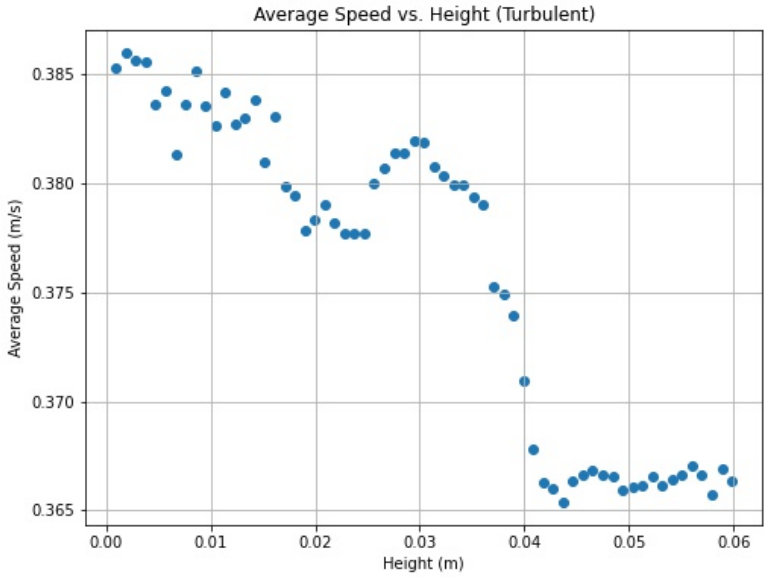

Figure 29: Average Speed in Turbulent Flow with Respect to Height

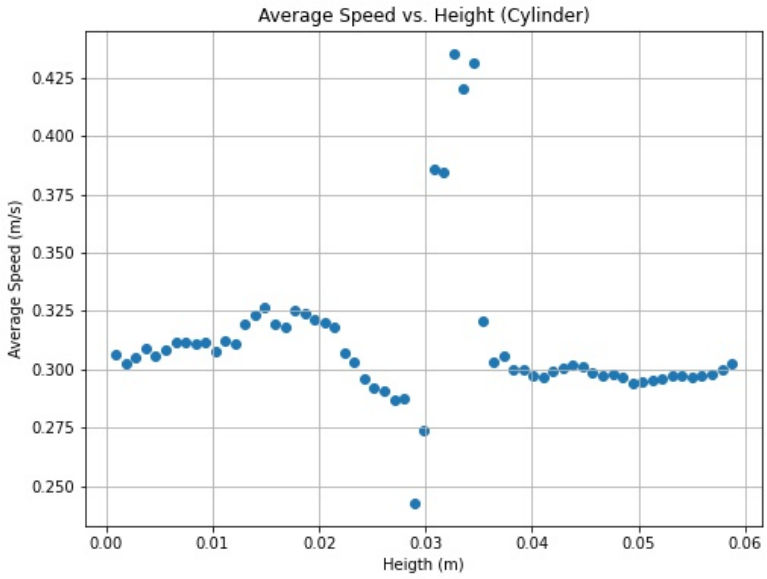

Figure 30: Average Speed in Laminar Flow with Respect to Height